ACS OMEGA

http://pubs.acs.org/journal/acsodf

Article

Carbonization of a Molybdenum Substrate Surface and Nanoparticles by a One-Step Method of Femtosecond Laser Ablation in a Hexane Solution

Yoshiki Tanaka, Xi Yu,* Shusaku Terakawa, Takafumi Ishida, Koh Saitoh, Hongwei Zhang, Toru Asaka, Fumihiro Itoigawa, Makoto Kuwahara, and Shingo Ono*

Cite This: *ACS Omega* 2023, 8, 7932−7939

Read Online

ACCESS | Metrics & More | Article Recommendations

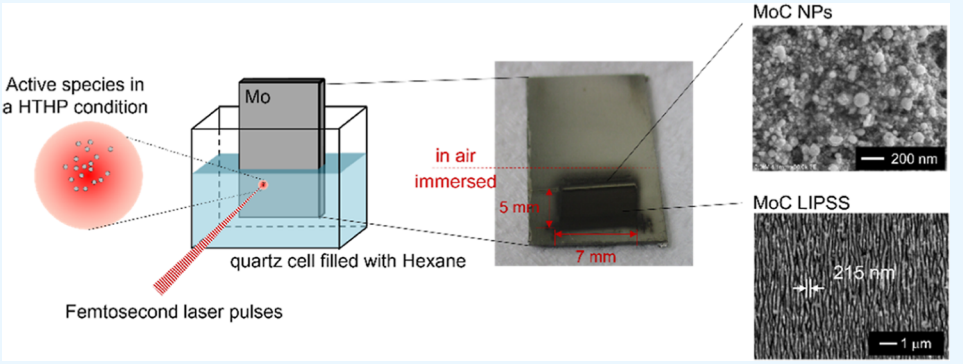

ABSTRACT: Molybdenum carbides (MoC and Mo_2C) are being reported for various applications, for example, catalysts for sustainable energies, nonlinear materials for laser applications, protective coatings for improving tribological performance, and so on. A one-step method for simultaneously fabricating molybdenum monocarbide (MoC) nanoparticles (NPs) and MoC surfaces with a laser-induced periodic surface structure (LIPSS) was developed by using pulsed laser ablation of a molybdenum (Mo) substrate in hexane. Spherical NPs with an average diameter of 61 nm were observed by scanning electron microscopy. The X-ray diffraction pattern and electron diffraction (ED) pattern results indicate that a face-centered cubic MoC was successfully synthesized for the NPs and on the laser-irradiated area. Notably, the ED pattern suggests that the observed NPs are nanosized single crystals, and a carbon shell was observed on the surface of MoC NPs. The X-ray diffraction pattern of both MoC NPs and LIPSS surface indicates the formation of FCC MoC, agreeing with the results of ED. The results of X-ray photoelectron spectroscopy also showed the bonding energy attributed to Mo−C, and the sp^2−sp^3 transition was confirmed on the LIPSS surface. The results of Raman spectroscopy have also supported the formation of MoC and amorphous carbon structures. This simple synthesis method for MoC may provide new possibilities for preparing Mo_xC-based devices and nanomaterials, which may contribute to the development of catalytic, photonic, and tribological fields.

1. INTRODUCTION

Energy storage and conversion technologies[1−3] are being developed, aiming at the realization of a sustainable human society.[4] Clean hydrogen fuel generated from water is one of the most friendly energies to the environment, and much attention is now paid to developing catalyst materials for the hydrogen evolution reaction (HER).[5] Platinum-group metals are reported as the best materials for electrocatalysts due to their optimal surface free energy, striking a balance between the adsorption and desorption of hydrogen during the HER.[6,7] However, these scarce and high-cost platinum-group metals need substitutes for the large-scale implementation and economic viability of HER-based technologies.[7] Molybdenum (Mo), as an alternative, is thousands of times that of platinum in the earth's crust,[8,9] and Mo-based materials have been reported for the potential of substituting platinum-based catalysts, such as MoS_2,[10−12] MoO_2,[13] MoP,[14−16] MoN,[17,18] and Mo_xC (molybdenum carbides, generally MoC and Mo_2C).[19−29] Furthermore, Mo_xC-based materials stand out for their catalytic performance, as well as their mechanical and chemical stabilities.[21,27−29] Besides, Mo_2C has also been

Received: December 2, 2022
Accepted: January 23, 2023
Published: February 13, 2023

reported for laser applications in the photonic field[30,31] and for improving the surface hardness and tribological performance of cutting tools.[32,33]

Most Mo_xC-based materials are fabricated in nanoparticles (NPs) using chemical syntheses, and ammonium pentamolybdate and organic solutions are used as Mo and carbon (C) resources, respectively.[19−26,28] Recently, direct carbonization of the Mo plate cathode was also reported using one-step electrodeposition.[29] With detailed process design and accurate adjustment of the precursor ratio and temperature, these mature technologies are exact synthesis methods for carbide nanomaterials. Pulsed laser ablation in liquids is also a flexible method to fabricate various NPs using bulk metal targets and solutions.[34−36] Moreover, femtosecond laser irradiation is a precision method of surface chemical modification,[37,38] which is becoming more and more efficient in precision surface processing, benefiting from the development of high-output lasers.[39,40] Franzel et al. reported the synthesis of multiphasic inhomogeneous Mo/MoC NPs by picosecond laser ablation of Mo foil in ethanol.[41] In this work, we irradiated a Mo substrate with a focused femtosecond laser beam in an oxygen-free organic hexane solution. This oxygen-free atmosphere can avoid Mo oxidation. Using this one-step method, we simultaneously achieved the carbonization of both the Mo substrate and Mo NPs and the formation of the MoC laser-induced periodic surface structure (LIPSS) on the laser-irradiated area. Additionally, the observed MoC NPs were confirmed as nanosized single crystals.

2. EXPERIMENTS AND METHODS

A molybdenum substrate (99.95%, Nilaco, Japan) was partly immersed in a quartz cell (size: 50 × 10 × 45 mm^3) filled with hexane (C_6H_{14} >96%, JIS K 8848, Kanto Chemical, Japan) and adhered to a two-axis motorized stage. The plate was then irradiated by femtosecond laser pulses from a Yb fiber laser, operating at a wavelength of 1045 nm, a pulse width of 700 fs, and a repetition rate of 100 kHz (D1000, IMRA America Inc., USA). The laser beam was focused on the substrate using an objective lens (RMS4X, Olympus Co., Japan) with a fluence of 2.23 J/cm^2. As shown in Figure 1a, in the high-temperature−

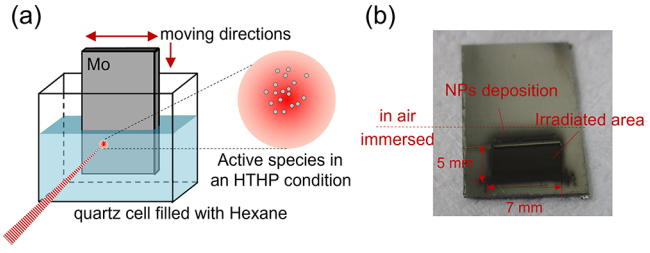

Figure 1. (a) Schematics of the experiment setup with an enlarged image of the laser ablation center; (b) Mo substrate after laser ablation in hexane.

high-pressure (HTHP) laser ablation center, active species of ions, atoms, and clusters ablated from Mo and hexane strongly reacted with each other to form metal carbide NPs, and the irradiated substrate surface also was carbonized simultaneously.[42−44] During laser ablation, the Mo substrate moved with a 2-axis motorized stage at a constant speed of 100 μm/s. This movement of the substrate can reduce the reabsorption of laser pulse by laser-induced plume and ensure the yield of NPs. The surface of the hexane solution lowered during laser ablation due to the volatility. The fresh C_6H_{14} solution was replenished little by little to ensure that laser ablation happened in the liquid atmosphere. The irradiated area was 5 mm × 7 mm (Figure 1b). The surface morphology of the laser-irradiated Mo substrate was characterized by scanning electron microscopy (SEM, SU6600, Hitachi, Japan). X-ray diffraction (SmartLab, Rigaku, Japan), Raman spectrum (NRS-3300 with an excitation laser wavelength of 532 nm, JASCO, Japan), and X-ray photoelectron spectroscopy (XPS, PHI5000 VersaProbe with an Al Kα anode) were performed to identify the compounds. The collected NPs were progressively analyzed by a scanning transmission electron microscope with an energy-dispersive X-ray spectroscope (JEM-ARM200F, JEOL, Japan).

3. RESULTS AND DISCUSSION

Discolorations were observed in the laser-irradiated area and its top, according to Figure 1b. Figure 2a shows the SEM image of the discolored area on top of the laser-irradiated area. Numerous spherical NPs were deposited in this area, and a considerable thickness compared to the diameter of NPs can be observed from cracks of deposition. The diffusion of laser-ablated NPs was observed during laser ablation. A part of the floating NPs were trapped on the surface of the hexane solution due to buoyancy. These NPs progressively aggregated to the NP deposition near the solution surface. The diameter distribution of the NPs deposited on the Mo substrate was obtained by measuring 300 particles from SEM images. The diameter is defined as the mean diameter of r_1 and r_2 shown in Figure 2a, and the directions of r_1 and r_2 are perpendicular to each other. With an average diameter of 61 nm, most of the particles are smaller than 100 nm, and some huge particles (>100 nm) can also be observed (Figure 2b). On the other hand, the formation of LIPSS was confirmed in the laser-irradiated area (Figure 2c). This periodic groove structure with a depth of up to several hundred nanometers can provide a higher surface-to-volume ratio, resulting in more possibility for forming active sites to enhance the catalytic performance.[45−47] The morphology of the LIPSS is controllable by the laser wavelength, polarization direction, laser fluence, and irradiated pulse number when laser-ablated in air.[47] In the case of laser ablation in liquid, these laser parameters can also affect the morphology. Additionally, a shorter wavelength will be induced in the liquid solution due to the higher refractive index than in the air, resulting in a shorter period.[48] For ultrashort pulse durations, multiphoton absorption of hexane can occur more easily, providing more carbon active racial to accelerate carbonization. Figure 2d plots the XRD pattern of the NP deposition and the irradiated and unprocessed substrate. All three measurements show facets of (1 1 0), (2 0 0), (2 1 1), and (2 2 0) originating from Mo. Additional molybdenum monocarbide (MoC) XRD peaks with facets of (1 1 1), (2 0 0), (2 2 0), and (2 2 2) were observed, revealing the carbonization of both the irradiated substrate and the deposited NPs. The XRD results also suggested the formation of α-MoC with a face-centered cubic (FCC) structure.[49]

Figure 3 displays the chemical-bonding state of Mo, C, and O (oxygen from the surface oxide layer) in the composites measured by XPS. Peaks in the XPS spectrum were fitted by using a mixed Gaussian/Lorentzian function, and the background was treated by the Shirley method. Table 1 shows the details of peak components. O 1s peaks assigned to molybdenum oxides (MoO_x) and the C═O bond were

https://doi.org/10.1021/acsomega.2c07697
ACS Omega 2023, 8, 7932−7939

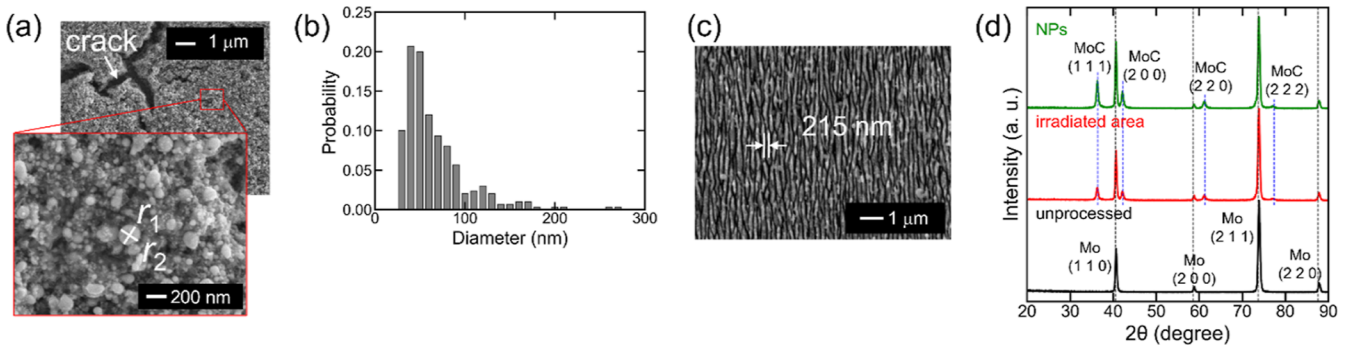

Figure 2. (a) SEM images of NP deposition, (b) diameter distribution of NPs deposited on the Mo substrate, (c) SEM image of the laser-irradiated Mo substrate surface, (d) XRD patterns of the unprocessed Mo substrate, laser-irradiated area, and NP deposition. Mo and MoC peaks were identified by referencing the ICDD-PDF no. 00-042-1120 (black dashed line) and no. 00-042-1120 (blue dashed line), respectively.

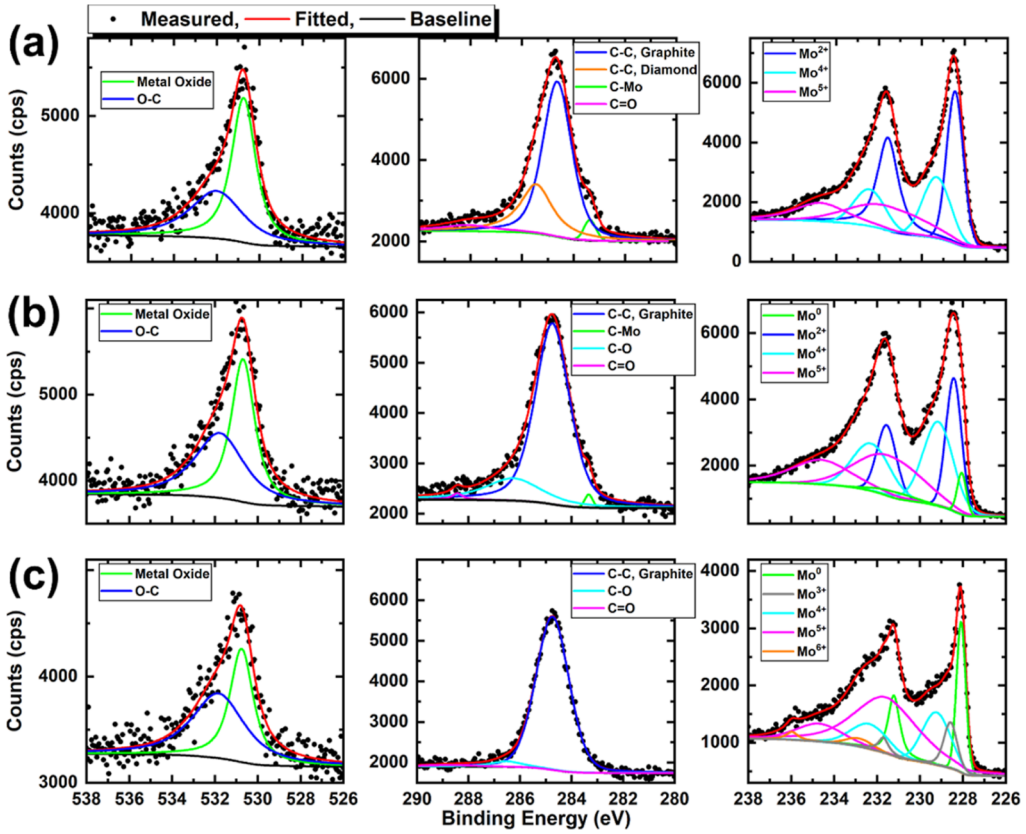

Figure 3. Results of XPS measurement. (a) Laser-ablated area, (b) NP deposition, and (c) unprocessed area. The measurement targets were preprocessed using Ar ion etching to reduce surface contamination.

observed for all three measurements.[50−52] Before laser processing, the samples were immersed in acetone and purified water for 5 min of ultrasonic cleaning, respectively. The presence of oxygen should be caused by exposure to the oxygen-containing atmosphere.[29] The main peak assigned to the C−C bond of sp^2 originating from graphite was observed for all three areas in the C 1s spectra, as well as C−O and C═O bonds originating from surface contaminations.[50,53−55] An additional Mo−C bond of C 1s was observed except for the measurement of the unprocessed area, indicating the carbonization for both NP deposition and the substrate surface. Interestingly, the C−C bond of sp^3 originating from the diamond located at 285.4 eV was detected for the laser-irradiated area,[53] revealing that the graphite−diamond transition happened under the HTHP conditions.[56−60] Generally, the laser ablation center has high pressure in the GPa range and a high temperature of several thousand degrees K.[61,62] A liquid-confined condition will induce a higher pressure and a longer laser shock duration which are more beneficial to the graphite−diamond transition.[43,60,62,63] Moreover, the stress on NPs could be released to the solution, and the unmovable substrate side will experience a higher pressure.

The Mo 3d spectrum consists of two peaks because of different electronic spins, assigned to Mo $3d_{5/2}$ and Mo $3d_{3/2}$, which are separated by 3.13 eV and have an area ratio of 3:2. Peaks of Mo^0, Mo^{3+}, Mo^{4+}, Mo^{5+}, and Mo^{6+} were observed for the unprocessed area. Mo^0 originates from the native Mo substrate.[50,64,65] Mo^{3+}, Mo^{4+}, Mo^{5+}, and Mo^{6+} originated from the molybdenum oxides[50,64,65] Mo_2O_3, MoO_2, Mo_2O_5, and MoO_3, respectively. These molybdenum oxides correspond to

https://doi.org/10.1021/acsomega.2c07697
ACS Omega 2023, 8, 7932−7939

Table 1. Fitting Details of Peak Components

		unprocessed		NPs		ablated	
		B. E. (eV)	Ratio (%)	B. E. (eV)	Ratio (%)	B. E. (eV)	Ratio (%)
C 1s	C−Mo			283.33	0.3	283.36	0.8
	sp^2	284.74	28.5	284.74	18.7	284.63	17.6
	sp^3					285.44	7.8
	C−O	286.51	1.2	286.26	4.4		
	C═O	288.67	0.4	288.44	0.3	288.10	1.6
O 1s	O−Mo	530.75	8.7	530.68	8.3	530.74	8.0
	O═C	531.83	11.2	531.77	8.0	532.00	5.8
Mo 3d	$Mo^0 3d_{5/2}$	228.08	6.2	228.05	1.7		
	Mo^0 $3d_{3/2}$	231.21	4.2	231.18	1.2		
	Mo^{2+} $3d_{5/2}$			228.42	9.6	228.45	14.1
	Mo^{2+} $3d_{3/2}$			231.55	6.4	231.58	9.4
	Mo^{3+}	228.58	3.1				
	Mo^{3+}	231.71	1.0				
	Mo^{4+} $3d_{5/2}$	229.23	6.5	229.15	12.3	229.31	9.8
	Mo^{4+} $3d_{3/2}$	232.36	4.3	232.28	8.2	232.44	6.5
	Mo^{5+} $3d_{5/2}$	231.56	18.7	231.47	12.4	231.58	11.2
	Mo^{5+} $3d_{3/2}$	234.69	4.3	234.60	8.2	234.71	7.5
	Mo^{6+} $3d_{5/2}$	232.83	0.9				
	Mo^{6+} $3d_{3/2}$	235.96	0.6				

the surface oxidation layer due to their exposure to the oxygen-containing atmosphere. After laser ablation, the Mo^0 peak ratio (peak area to the area summary) decreases to 2.9% from the initial 10.4% (unprocessed area) for the NP deposition and progressively to zero for the laser-ablated area. The remaining Mo^0 peak in the NP XPS spectrum reveals the incomplete carbonization of some large Mo species ablated from the substrate during laser processing,[36] and the absence of the Mo^0 peak for the laser-ablated area suggests that the substrate side is covered entirely by carbides or oxides. On the contrary, the peak attributed to Mo^{2+} corresponding to the Mo−C bond was observed for the NP deposition with a peak ratio of 16%, and this peak ratio increased to 23.5% for the laser-ablated area. Associating with the increase of the C 1s peak of the Mo−C bond from 0.3 to 0.8% of NP deposition to the laser-ablated area, the substrate side showed more complete carbonization than the NP deposition.

The Raman spectra of the laser-ablated area, NP deposition, and Mo substrate were also measured to evaluate the surface state (Figure 4). Another Mo substrate covered with several drops of hexane was evaluated from the Raman spectra as a reference. These hexane droplets were evaporated naturally before Raman spectrum measurement. The peaks located at around 1350 and 1600 cm^{-1} originated from the disordered carbon phase and graphite of amorphous carbon (a-C), respectively,[66−69] revealing the formation of a-C on the laser-irradiated area and NP deposition. Very weak peaks located at around 660, 820, and 995 cm^{-1} were observed for the Raman spectra of the laser-ablated area and NP deposition, which can be attributed to the characteristic peaks of MoO_3 or Mo_2C.[70−72] However, these three peaks were not observed for the Mo substrate, suggesting that the surface molybdenum oxide contaminations are not detectable in the Raman measurement. These three weak peaks should have originated from Mo−C modes, revealing the formation of MoC.[73]

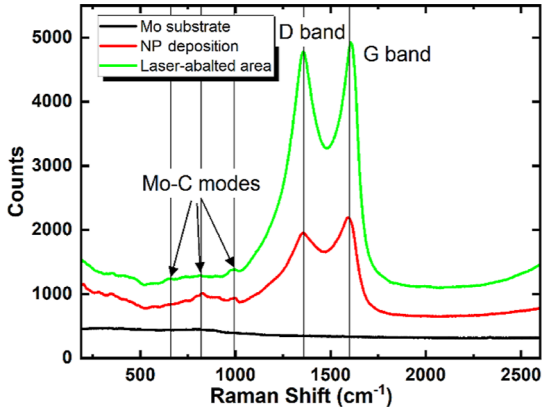

Figure 4. Raman spectrum of the laser-ablated area, NP deposition, and Mo substrate surface.

The NP deposition was removed from the substrate by using a spatula and collected in a glass sampling bottle with ethanol. The NPs were then dispersed in an ethanol solution using the agitation induced using an ultrasonic cleaning machine. A part of the collected NPs in ethanol solution were added dropwise onto a microgrid with the ethanol solution. After natural evaporation of ethanol, these NPs were analyzed by STEM−EDX. Figure 5a displays the bright-field (BF) image of the NPs, and (b−d) are elemental mappings of Mo, C, and O by EDX, respectively. Most of the NPs in the aggregation shown in Figure 5a have a size of less than 100 nm, except a large particle with a size larger than 100 nm. Regardless of particle size, Mo and C are almost uniformly distributed in these NPs. The Mo mapping has the clearest outline and almost perfectly reflects the shape of NPs, and the C distribution slightly exudes the shape of NPs. On the contrary, O is indistinct. These elemental mappings suggest that these collected NPs were uniformly carbonized. The TEM diffraction patterns of area 1 and area 2 (marked in Figure 5a) are displayed in Figure 5e,f, respectively. Both area 1 and area 2 display a diffraction pattern of a FCC MoC, which are observed from the axis of ⟨1 1 0⟩ and ⟨1 2 1⟩, respectively. The intensity profiles of area 1 and area 2 transformed from their diffraction pattern are shown in Figure 5g.[74] These intensity profiles match very well with the XRD patterns, as shown in Figure 2d. These results indicate

https://doi.org/10.1021/acsomega.2c07697
ACS Omega 2023, 8, 7932−7939

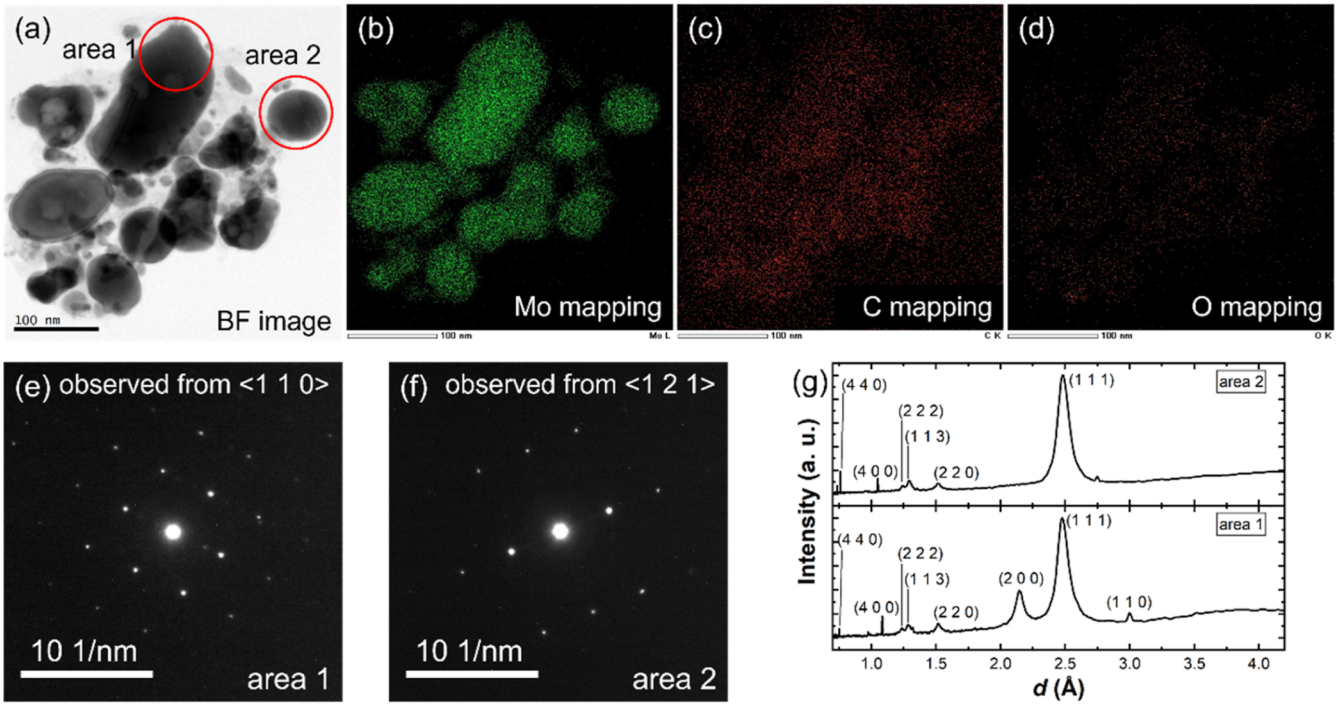

Figure 5. (a) BF image of MoC NP aggregation; (b–d) Mo, C, and O mappings; (e–f) ED pattern of two NPs as marked in (a,g) and the intensity profiles transformed from the diffraction pattern of (e,f), in which the horizontal axis is the inverse of the distance from the central peak to each peak, i.e., lattice spacing.

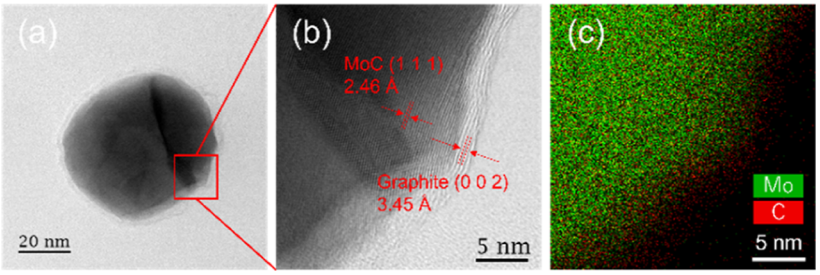

Figure 6. (a) BF image of an individual MoC NP, (b) enlarged image of (a), and (c) EDX mapping of (b).

the formation of nanosized MoC single crystals, as marked in area 1 and area 2. Also, as a kind of photocatalyst,[75] high crystallinity can mitigate the recombination of electron–hole pairs, therefore enhancing the catalytic performance.

An individual MoC NP was also observed by TEM. Figure 6a is the BF image of an individual particle. This NP has a core–shell structure, with a shell of less than 4 nm. As shown in the enlarged TEM image (Figure 6b), the core part has a lattice fringe of 2.46 Å corresponding to the FCC MoC with the direction of ⟨1 1 1⟩. Figure 5c displays the EDX mapping of this particle. Similar to the mapping results shown in Figure 5, this NP has a slightly exuded C distribution corresponding to the shell structure. The core–shell structure has also been reported by Hu et al. in their experiment of laser ablation of iron in organic liquids, resulting in the synthesis of NPs with diamond-like carbon shells.[76] Nevertheless, the shell structure in this particle showed an amorphous feature. Part of the shell has a layer structure with a layer distance of 3.45 Å corresponding to the lattice distance of graphite,[77] which is also confirmed by our XPS measurement (Figure 3) and Raman spectra (Figure 4). Covering the core of the catalyst with a carbon shell has been reported as a strategy to improve the catalytic performance.[78] Carbon shells with suitable thickness and crystallinity can trigger the catalytic reaction on the shell surface using electrons transferred from the core of the catalyst and work as a protection to improve the stability of encapsulated catalysts during the catalytic reaction. On the other hand, this shell structure may hinder the direct contact between reactants and NPs, leading to the weakening of catalytic performance. Nevertheless, similar graphitic and amorphous carbon shells were reported with improved catalyst performance on metal electrocatalysts.[79]

4. CONCLUSIONS

By using a one-step method of laser ablation on the Mo substrate in hexane, we simultaneously achieved (1) the carbonization of Mo NPs and the Mo substrate surface, (2) an MoC LIPSS with an improved surface-to-volume ratio from a flat surface, (3) a graphite and amorphous carbon shell structure on the surface of MoC NPs. This simple synthesis method for MoC may provide a new choice for the preparation of Mo_xC-based devices and nanomaterials, which can accelerate the revolution of replacing noble-metal-based catalysts with more economical Mo-based catalysts.

https://doi.org/10.1021/acsomega.2c07697
ACS Omega 2023, 8, 7932–7939

AUTHOR INFORMATION

Corresponding Authors

Xi Yu − *Institute of Materials and Systems for Sustainability, Nagoya University, Nagoya 464-8601, Japan;* orcid.org/0000-0002-4517-7905; Email: x.yu@imass.nagoya-u.ac.jp

Shingo Ono − *Department of Physical Science and Engineering, Nagoya Institute of Technology, Nagoya 466-8555, Japan*; Email: ono.shingo@nitech.ac.jp

Authors

Yoshiki Tanaka − *Department of Physical Science and Engineering, Nagoya Institute of Technology, Nagoya 466-8555, Japan*

Shusaku Terakawa − *Department of Physical Science and Engineering, Nagoya Institute of Technology, Nagoya 466-8555, Japan*

Takafumi Ishida − *Institute of Materials and Systems for Sustainability, Nagoya University, Nagoya 464-8601, Japan; Graduate School of Engineering, Nagoya University, Nagoya 464-8603, Japan*

Koh Saitoh − *Institute of Materials and Systems for Sustainability, Nagoya University, Nagoya 464-8601, Japan; Graduate School of Engineering, Nagoya University, Nagoya 464-8603, Japan*

Hongwei Zhang − *Biogas Institute of Ministry of Agriculture and Rural Affairs, Chengdu 610042, China*

Toru Asaka − *Life Science and Applied Chemistry Advanced Ceramics, Nagoya Institute of Technology, Nagoya 466-8555, Japan;* orcid.org/0000-0001-7399-1077

Fumihiro Itoigawa − *Department of Electrical and Mechanical Engineering, Nagoya Institute of Technology, Nagoya 466-8555, Japan*

Makoto Kuwahara − *Graduate School of Engineering, Nagoya University, Nagoya 464-8603, Japan;* orcid.org/0000-0003-0046-5716

Complete contact information is available at: https://pubs.acs.org/10.1021/acsomega.2c07697

Funding

This study was sponsored by the Amada Foundation (grant no. AF-2019213-B2); Iketani Science and Technology Foundation (grant no. 0341176 A); Strategic Foundational Technology Improvement Support Operation; Grants-in-aid for the Program for Building Regional Innovation Ecosystem "Aichi Innovation Ecosystem Project for Next-Generation Automobile" from the Ministry of Education, Culture, Sports, Science and Technology of Japan; Osawa Scientific Studies Grants Foundation; KAKENHI (grant no. 21H04637); and Hirose Foundation.

Notes

The authors declare no competing financial interest.

The data that support the findings of this study are available from the corresponding author upon reasonable request.

REFERENCES

(1) Kudo, A.; Miseki, Y. Heterogeneous Photocatalyst Materials for Water Splitting. *Chem. Soc. Rev.* **2009**, *38*, 253−278.

(2) Chapin, D. M.; Fuller, C. S.; Pearson, G. L. A New Silicon p-n Junction Photocell for Converting Solar Radiation into Electrical Power. *J. Appl. Phys.* **1954**, *25*, 676−677.

(3) Tsuchiya, T.; Takayanagi, M.; Mitsuishi, K.; Imura, M.; Ueda, S.; Koide, Y.; Higuchi, T.; Terabe, K. The Electric Double Layer Effect and Its Strong Suppression at Li+ Solid Electrolyte/Hydrogenated Diamond Interfaces. *Commun. Chem.* **2021**, *4*, 1−11.

(4) Chu, S.; Majumdar, A. Opportunities and Challenges for a Sustainable Energy Future. *Nature* **2012**, *488*, 294−303.

(5) Vesborg, P. C. K.; Seger, B.; Chorkendorff, I. Recent Development in Hydrogen Evolution Reaction Catalysts and Their Practical Implementation. *J. Phys. Chem. Lett.* **2015**, *6*, 951−957.

(6) Nørskov, J. K.; Bligaard, T.; Logadottir, A.; Kitchin, J. R.; Chen, J. G.; Pandelov, S.; Stimming, U. Trends in the Exchange Current for Hydrogen Evolution. *J. Electrochem. Soc.* **2005**, *152*, J23.

(7) Rhatigan, S.; Michel, M.-C.; Nolan, M. Hydrogen Evolution on Non-Metal Oxide Catalysts. *J. Phys.: Energy* **2020**, *2*, 042002.

(8) Hans Wedepohl, K. The Composition of the Continental Crust. *Geochim. Cosmochim. Acta* **1995**, *59*, 1217−1232.

(9) Yaroshevsky, A. A. Abundances of chemical elements in the Earth's crust. *Geochem. Int.* **2006**, *44*, 48−55.

(10) Li, H.; Tsai, C.; Koh, A. L.; Cai, L.; Contryman, A. W.; Fragapane, A. H.; Zhao, J.; Han, H. S.; Manoharan, H. C.; Abild-Pedersen, F.; Nørskov, J. K.; Zheng, X. Activating and Optimizing MoS2 Basal Planes for Hydrogen Evolution through the Formation of Strained Sulphur Vacancies. *Nat. Mater.* **2016**, *15*, 48−53.

(11) Benck, J. D.; Hellstern, T. R.; Kibsgaard, J.; Chakthranont, P.; Jaramillo, T. F. Catalyzing the Hydrogen Evolution Reaction (HER) with Molybdenum Sulfide Nanomaterials. *ACS Catal.* **2014**, *4*, 3957−3971.

(12) Chen, S.; Duan, J.; Tang, Y.; Jin, B.; Zhang Qiao, S. Molybdenum Sulfide Clusters-Nitrogen-Doped Graphene Hybrid Hydrogel Film as an Efficient Three-Dimensional Hydrogen Evolution Electrocatalyst. *Nano Energy* **2015**, *11*, 11−18.

(13) Jin, Y.; Wang, H.; Li, J.; Yue, X.; Han, Y.; Shen, P. K.; Cui, Y. Porous MoO 2 Nanosheets as Non-noble Bifunctional Electrocatalysts for Overall Water Splitting. *Adv. Mater.* **2016**, *28*, 3785−3790.

(14) Kibsgaard, J.; Jaramillo, T. F. Molybdenum Phosphosulfide: An Active, Acid-Stable, Earth-Abundant Catalyst for the Hydrogen Evolution Reaction. *Angew. Chem., Int. Ed.* **2014**, *53*, 14433−14437.

(15) McEnaney, J. M.; Crompton, J.; Callejas, J. F.; Popczun, E. J.; Biacchi, A. J.; Lewis, N. S.; Schaak, R. E. Amorphous Molybdenum Phosphide Nanoparticles for Electrocatalytic Hydrogen Evolution. *Chem. Mater.* **2014**, *26*, 4826−4831.

(16) Xing, Z.; Liu, Q.; Asiri, A. M.; Sun, X. Closely Interconnected Network of Molybdenum Phosphide Nanoparticles: A Highly Efficient Electrocatalyst for Generating Hydrogen from Water. *Adv. Mater.* **2014**, *26*, 5702−5707.

(17) Chen, W. F.; Sasaki, K.; Ma, C.; Frenkel, A. I.; Marinkovic, N.; Muckerman, J. T.; Zhu, Y.; Adzic, R. R. Hydrogen-Evolution Catalysts Based on Non-Noble Metal Nickel-Molybdenum Nitride Nanosheets. *Angew. Chem., Int. Ed.* **2012**, *51*, 6131−6135.

(18) Cao, B.; Veith, G. M.; Neuefeind, J. C.; Adzic, R. R.; Khalifah, P. G. Mixed Close-Packed Cobalt Molybdenum Nitrides as Non-Noble Metal Electrocatalysts for the Hydrogen Evolution Reaction. *J. Am. Chem. Soc.* **2013**, *135*, 19186−19192.

(19) Chen, W.-F.; Wang, C.-H.; Sasaki, K.; Marinkovic, N.; Xu, W.; Muckerman, J. T.; Zhu, Y.; Adzic, R. R. Highly Active and Durable Nanostructured Molybdenum Carbide Electrocatalysts for Hydrogen Production. *Energy Environ. Sci.* **2013**, *6*, 943.

(20) Pan, L.; Li, Y.; Yang, S.; Liu, P.; Yu, M.; Yang, H. Molybdenum Carbide Stabilized on Graphene with High Electrocatalytic Activity for Hydrogen Evolution Reaction. *Chem. Commun.* **2014**, *50*, 13135−13137.

(21) Li, C.; Wang, Z.; Liu, M.; Wang, E.; Wang, B.; Xu, L.; Jiang, K.; Fan, S.; Sun, Y.; Li, J.; Liu, K. Ultrafast Self-Heating Synthesis of Robust Heterogeneous Nanocarbides for High Current Density Hydrogen Evolution Reaction. *Nat. Commun.* **2022**, *13*, 1−11.

(22) Liao, L.; Wang, S.; Xiao, J.; Bian, X.; Zhang, Y.; Scanlon, M. D.; Hu, X.; Tang, Y.; Liu, B.; Girault, H. H. A Nanoporous Molybdenum Carbide Nanowire as an Electrocatalyst for Hydrogen Evolution Reaction. *Energy Environ. Sci.* **2014**, *7*, 387−392.

(23) Tang, C.; Sun, A.; Xu, Y.; Wu, Z.; Wang, D. High Specific Surface Area Mo2C Nanoparticles as an Efficient Electrocatalyst for Hydrogen Evolution. *J. Power Sources* **2015**, *296*, 18−22.
(24) Huang, Y.; Gong, Q.; Song, X.; Feng, K.; Nie, K.; Zhao, F.; Wang, Y.; Zeng, M.; Zhong, J.; Li, Y. Mo2C Nanoparticles Dispersed on Hierarchical Carbon Microflowers for Efficient Electrocatalytic Hydrogen Evolution. *ACS Nano* **2016**, *10*, 11337−11343.
(25) Mu, Y.; Zhang, Y.; Fang, L.; Liu, L.; Zhang, H.; Wang, Y. Controllable Synthesis of Molybdenum Carbide Nanoparticles Embedded in Porous Graphitized Carbon Matrixes as Efficient Electrocatalyst for Hydrogen Evolution Reaction. *Electrochim. Acta* **2016**, *215*, 357−365.
(26) Guo, J.; Wang, J.; Wu, Z.; Lei, W.; Zhu, J.; Xia, K.; Wang, D. Controllable Synthesis of Molybdenum-Based Electrocatalysts for a Hydrogen Evolution Reaction. *J. Mater. Chem. A* **2017**, *5*, 4879−4885.
(27) Li, J.-S.; Wang, Y.; Liu, C. H.; Li, S. L.; Wang, Y. G.; Dong, L. Z.; Dai, Z. H.; Li, Y. F.; Lan, Y. Q. Coupled Molybdenum Carbide and Reduced Graphene Oxide Electrocatalysts for Efficient Hydrogen Evolution. *Nat. Commun.* **2016**, *7*, 11204.
(28) Wang, D.; Wang, J.; Luo, X.; Wu, Z.; Ye, L. In Situ Preparation of Mo2C Nanoparticles Embedded in Ketjenblack Carbon as Highly Efficient Electrocatalysts for Hydrogen Evolution. *ACS Sustainable Chem. Eng.* **2018**, *6*, 983−990.
(29) Liu, W.; Wang, X.; Wang, F.; Du, K.; Zhang, Z.; Guo, Y.; Yin, H.; Wang, D. A durable and pH-universal self-standing MoC-Mo2C heterojunction electrode for efficient hydrogen evolution reaction. *Nat. Commun.* **2021**, *12*, 6776.
(30) Liu, S.; Lu, J.; Huang, H.; Xu, N.; Qu, J.; Wen, Q. Ultrafast Photonics Applications Based on Evanescent Field Interactions with 2D Molybdenum Carbide (Mo2C). *J. Mater. Chem. C* **2021**, *9*, 6187−6192.
(31) Liu, S.; Cui, N.; Liu, S.; Wang, P.; Dong, L.; Chen, B.; Zhang, N.; Zhang, K.; Wang, Y. Nonlinear Optical Properties and Passively Q-Switched Laser Application of a Layered Molybdenum Carbide at 639 Nm. *Opt. Lett.* **2022**, *47*, 1830.
(32) Kuleshov, A. K.; Uglov, V. V.; Rusalsky, D. P. Hard and Wear-Resistant Niobium, Molybdenum Carbide Layered Coatings on WC-Co Tools Produced by Ion Bombardment and Cathodic Vacuum Arc Deposition. *Surf. Coat. Technol.* **2020**, *395*, 125920.
(33) Martínez, E.; Wiklund, U.; Esteve, J.; Montalà, F.; Carreras, L. L. Tribological Performance of TiN Supported Molybdenum and Tantalum Carbide Coatings in Abrasion and Sliding Contact. *Wear* **2002**, *253*, 1182−1187.
(34) Balachandran, A.; Sreenilayam, S. P.; Madanan, K.; Thomas, S.; Brabazon, D. Nanoparticle Production via Laser Ablation Synthesis in Solution Method and Printed Electronic Application - A Brief Review. *Results Eng.* **2022**, *16*, 100646.
(35) Kim, M.; Osone, S.; Kim, T.; Higashi, H.; Seto, T. Synthesis of Nanoparticles by Laser Ablation: A Review. *KONA Powder Part. J.* **2017**, *34*, 80−90.
(36) Yu, X.; Terakawa, S.; Hayashi, S.; Asaka, T.; Itoigawa, F.; Ono, S.; Takayanagi, J. Carbonization of Silicon Nanoparticles via Ablation Induced by Femtosecond Laser Pulses in Hexane. *Arabian J. Sci. Eng.* **2017**, *42*, 4221−4226.
(37) Bäuerle, D. *Laser Processing and Chemistry*; Springer Berlin Heidelberg: Berlin, Heidelberg, 2011.
(38) Liu, X.; Tanaka, Y.; Fujiwara, S.; Maegawa, S.; Ono, S.; Itoigawa, F. Surface Modification Technique of Titanium Alloy to Improve the Tribological Properties Using Sub-Ns Laser Irradiation in PAO Oil. *J. Adv. Mech. Des. Syst. Manuf.* **2023**, *17*, JAMDSM0014.
(39) Mans, T.; Dolkemeyer, J.; Schnitzler, C. High Power Femtosecond Lasers. *Laser Tech. J.* **2014**, *11*, 40−43.
(40) Bernard, O.; Audouard, E.; Schöps, B.; Delaigue, M.; Dalla-Barba, G.; Mishchik, K.; Hönninger, C.; Mottay, E. Efficient Micro Processing with High Power Femtosecond Lasers by Beam Engineering and Modelling. *Procedia CIRP* **2018**, *74*, 310−314.
(41) Franzel, L.; Phumisithikul, K.; Bertino, M. F.; Carpenter, E. E. Synthesis of Multiphasic Inhomogeneous Mo/MoC Nanoparticles by Pulsed Laser Ablation. *J. Nanoparticle Res.* **2013**, *15*, 2032.
(42) Abdolvand, A.; Khan, S. Z.; Yuan, Y.; Crouse, P. L.; Schmidt, M. J. J.; Sharp, M.; Liu, Z.; Li, L. Generation of Titanium-Oxide Nanoparticles in Liquid Using a High-Power, High-Brightness Continuous-Wave Fiber Laser. *Appl. Phys. A: Mater. Sci. Process.* **2008**, *91*, 365−368.
(43) Fabbro, R.; Fournier, J.; Ballard, P.; Devaux, D.; Virmont, J. Physical study of laser-produced plasma in confined geometry. *J. Appl. Phys.* **1990**, *68*, 775−784.
(44) Berthe, L.; Fabbro, R.; Peyre, P.; Tollier, L.; Bartnicki, E. Shock Waves from a Water-Confined Laser-Generated Plasma. *J. Appl. Phys.* **1997**, *82*, 2826−2832.
(45) Lange, K.; Schulz-Ruhtenberg, M.; Caro, J. Platinum Electrodes for Oxygen Reduction Catalysis Designed by Ultrashort Pulse Laser Structuring. *Chemelectrochem* **2017**, *4*, 570−576.
(46) Neale, A. R.; Jin, Y.; Ouyang, J.; Hughes, S.; Hesp, D.; Dhanak, V.; Dearden, G.; Edwardson, S.; Hardwick, L. J. Electrochemical Performance of Laser Micro-Structured Nickel Oxyhydroxide Cathodes. *J. Power Sources* **2014**, *271*, 42−47.
(47) Bonse, J.; Hohm, S.; Kirner, S. V.; Rosenfeld, A.; Kruger, J. Laser-Induced Periodic Surface Structures- A Scientific Evergreen. *IEEE J. Sel. Top. Quantum Electron.* **2017**, *23*, 1−59.
(48) Albu, C.; Dinescu, A.; Filipescu, M.; Ulmeanu, M.; Zamfirescu, M. Periodical Structures Induced by Femtosecond Laser on Metals in Air and Liquid Environments. *Appl. Surf. Sci.* **2013**, *278*, 347−351.
(49) Clougherty, E. V.; Lothrop, K. H.; Kafalas, J. A. A New Phase Formed by High-Pressure Treatment : Face-Centred Cubic Molybdenum Monocarbide. *Nature* **1961**, *191*, 1194.
(50) Moulder, J. F. In *Handbook of X-ray Photoelectron Spectroscopy: A Reference Book of Standard Spectra for Identification and Interpretation of XPS Data*; Chastain, J., Ed.; Physical Electronics Division, PerkinElmer Corporation, 1992.
(51) Zhang, Q.; Pastor-Pérez, L.; Jin, W.; Gu, S.; Reina, T. R. Understanding the Promoter Effect of Cu and Cs over Highly Effective β-Mo2C Catalysts for the Reverse Water-Gas Shift Reaction. *Appl. Catal., B* **2019**, *244*, 889−898.
(52) Scanlon, D. O.; Watson, G. W.; Payne, D. J.; Atkinson, G. R.; Egdell, R. G.; Law, D. S. L. Theoretical and Experimental Study of the Electronic Structures of MoO3and MoO2. *J. Phys. Chem. C* **2010**, *114*, 4636−4645.
(53) Kloprogge, J. T.; Wood, B. J. *Handbook of Mineral Spectroscopy X-ray Photoelectron Spectra*; Elsevier, 2020; Vol. *1*.
(54) Yoon, S. F.; Huang, Q. F.; Rusli; Yang, H.; Ahn, J.; Zhang, Q.; Blomfield, C.; Tielsch, B.; Tan, L. Y. C. X-Ray Photoelectron Spectroscopy of Molybdenum-Containing Carbon Films. *J. Appl. Phys.* **1999**, *86*, 4871−4875.
(55) Chen, M.; Song, C.; Liang, C.; Zhang, B.; Sun, Y.; Li, S.; Lin, L.; Xu, P. Crystalline Phase Induced Raman Enhancement on Molybdenum Carbides. *Inorg. Chem. Front.* **2022**, *9*, 2575−2582.
(56) Bundy, F. P. Direct Conversion of Graphite to Diamond in Static Pressure Apparatus. *J. Chem. Phys.* **1963**, *38*, 631−643.
(57) Naka, S.; Horii, K.; Takeda, Y.; Hanawa, T. Direct Conversion of Graphite to Diamond under Static Pressure. *Nature* **1976**, *259*, 38−39.
(58) DeCarli, P. S.; Jamieson, J. C. Formation of Diamond by Explosive Shock. *Science* **1961**, *133*, 1821−1822.
(59) Irifune, T.; Kurio, A.; Sakamoto, S.; Inoue, T.; Sumiya, H. Ultrahard Polycrystalline Diamond from Graphite. *Nature* **2003**, *421*, 599−600.
(60) Marcu, A.; Avotina, L.; Marin, A.; Lungu, C. P.; Grigorescu, C. E. A.; Demitri, N.; Ursescu, D.; Porosnicu, C.; Osiceanu, P.; Kizane, G.; Grigoriu, C. Laser Irradiation of Carbon-Tungsten Materials. *J. Phys. D: Appl. Phys.* **2014**, *47*, 355305.
(61) Berthe, L.; Fabbro, R.; Peyre, P.; Bartnicki, E. Wavelength Dependent of Laser Shock-Wave Generation in the Water-Confinement Regime. *J. Appl. Phys.* **1999**, *85*, 7552−7555.
(62) Bonelli, M.; Miotello, A.; Ossi, P.; Pessi, A.; Gialanella, S. Laser-Irradiation-Induced Structural Changes on Graphite. *Phys. Rev. B: Condens. Matter Mater. Phys.* **1999**, *59*, 13513−13516.

https://doi.org/10.1021/acsomega.2c07697
ACS Omega 2023, 8, 7932−7939

(63) Mundy, C. J.; Curioni, A.; Goldman, N.; Will Kuo, I.-F.; Reed, E. J.; Fried, L. E.; Ianuzzi, M. Ultrafast Transformation of Graphite to Diamond: An Ab Initio Study of Graphite under Shock Compression. *J. Chem. Phys.* **2008**, *128*, 184701.
(64) Lu, Y. C.; Clayton, C. R. An XPS Study of the Passive and Transpassive Behavior of Molybdenum in Deaerated 0.1 M HCl. *Corros. Sci.* **1989**, *29*, 927−937.
(65) McIntyre, N. S.; Johnston, D. D.; Coatsworth, L. L.; Davidson, R. D.; Brown, J. R. X-Ray Photoelectron Spectroscopic Studies of Thin Film Oxides of Cobalt and Molybdenum. *Surf. Interface Anal.* **1990**, *15*, 265−272.
(66) Ferrari, A. C.; Rodil, S. E.; Robertson, J. Interpretation of Infrared and Raman Spectra of Amorphous Carbon Nitrides. *Phys. Rev. B* **2003**, *67*, 155306.
(67) Liu, X.; Natsume, K.; Maegawa, S.; Itoigawa, F. Improvement of Crystallization in CVD Diamond Coating Induced by Femtosecond Laser Irradiation. *Diam. Relat. Mater.* **2020**, *107*, 107883.
(68) Ferrari, A. C.; Robertson, J. Raman spectroscopy of amorphous, nanostructured, diamond-like carbon, and nanodiamond. *Philos. Trans. R. Soc., A* **2004**, *362*, 2477−2512.
(69) Ferrari, A. C.; Robertson, J. Origin of the1150−cm−1Raman mode in nanocrystalline diamond. *Phys. Rev. B* **2001**, *63*, 121405.
(70) Frauwallner, M.-L.; López-Linares, F.; Lara-Romero, J.; Scott, C. E.; Ali, V.; Hernández, E.; Pereira-Almao, P. Toluene Hydrogenation at Low Temperature Using a Molybdenum Carbide Catalyst. *Appl. Catal., A* **2011**, *394*, 62−70.
(71) Qiu, J.; Yang, Z.; Li, Q.; Li, Y.; Wu, X.; Qi, C.; Qiao, Q. Formation of N-Doped Molybdenum Carbide Confined in Hierarchical and Hollow Carbon Nitride Microspheres with Enhanced Sodium Storage Properties. *J. Mater. Chem. A* **2016**, *4*, 13296−13306.
(72) Gao, Q.; Zhang, C.; Xie, S.; Hua, W.; Zhang, Y.; Ren, N.; Xu, H.; Tang, Y. Synthesis of Nanoporous Molybdenum Carbide Nanowires Based on Organic−Inorganic Hybrid Nanocomposites with Sub-Nanometer Periodic Structures. *Chem. Mater.* **2009**, *21*, 5560−5562.
(73) Yang, Y.; Liu, X.; Xu, Y.; Gao, X.; Dai, Y.; Tang, Y. Palladium-Incorporated α-MoC Mesoporous Composites for Enhanced Direct Hydrodeoxygenation of Anisole. *Catalysts* **2021**, *11*, 370.
(74) Shi, H.; Luo, M.; Wang, W. ElectronDiffraction Tools, a DigitalMicrograph Package for Electron Diffraction Analysis. *Comput. Phys. Commun.* **2019**, *243*, 166−173.
(75) Zhou, Y.; Wang, W.; Zhang, C.; Huang, D.; Lai, C.; Cheng, M.; Qin, L.; Yang, Y.; Zhou, C.; Li, B.; Luo, H.; He, D. Sustainable Hydrogen Production by Molybdenum Carbide-Based Efficient Photocatalysts: From Properties to Mechanism. *Adv. Colloid Interface Sci.* **2020**, *279*, 102144.
(76) Hu, A.; Sanderson, J.; Zhou, Y.; Duley, W. W. Formation of Diamond-like Carbon by Fs Laser Irradiation of Organic Liquids. *Diam. Relat. Mater.* **2009**, *18*, 999−1001.
(77) Popova, A. N. Crystallographic Analysis of Graphite by X-Ray Diffraction. *Coke Chem.* **2017**, *60*, 361−365.
(78) Jang, J.-H.; Jeffery, A. A.; Min, J.; Jung, N.; Yoo, S. J. Emerging Carbon Shell-Encapsulated Metal Nanocatalysts for Fuel Cells and Water Electrolysis. *Nanoscale* **2021**, *13*, 15116−15141.
(79) Khani, H.; Grundish, N. S.; Wipf, D. O.; Goodenough, J. B. Graphitic-Shell Encapsulation of Metal Electrocatalysts for Oxygen Evolution, Oxygen Reduction, and Hydrogen Evolution in Alkaline Solution. *Adv. Energy Mater.* **2020**, *10*, 1903215.

https://doi.org/10.1021/acsomega.2c07697
ACS Omega 2023, 8, 7932−7939